

Effect of magnetic axis torsion and magnetic surfaces ellipticity on the rotational transform and the magnetic shear

S. Guinchard*

Section de Physique, Ecole Polytechnique Fédérale de Lausanne, Lausanne, Suisse

(Supervised by A. Baillod and J. Loizu)[†]

(Dated: January 12, 2022)

In this document, the torsion τ is introduced, and evaluated for some closed curves, as a toroidal helix. In this context, and assuming circular flux surfaces, the rotational transform ι is determined analytically on the magnetic axis using the result derived by Helander in [1]. Results are then verified by comparison with the Stepped Pressure Equilibrium Code (SPEC). Finally, flux surface ellipticity is introduced and combined with the magnetic axis torsion, and the magnetic shear s is reviewed for several torsion-ellipticity combinations.

Keywords: Stellarator, magnetic shear, rotational transform, iota, torsion, curvature, quasi-axisymmetric stellarator, ellipticity

I. INTRODUCTION

Stellarators, as tokamaks, are magnetic confinement devices that hold promises to confine plasmas with sufficient efficiency to achieve net production of electricity by nuclear fusion. Stellarators are toroidal infrastructures, since it has been shown by mean of topology, that in 3D-space, the possible shapes of magnetic surfaces formed by closed and non vanishing field lines, are limited to a torus. Contrarily to their cousins tokamaks, for which the poloidal magnetic field is produced by mean of a net toroidal plasma current, stellarators' magnetic fields are achieved by mean of external coils only. Therefore, many of the current-driven instabilities found in tokamaks are not excited in stellarators, which is one of their main advantages.

The rotational transform, ι , is considered an important parameter to take into account for plasma confinement [2, 3]. In Appendix.(A), an analytical development shows to what extent ι is crucial in the description of a screw pinch. Note that the safety factor, denoted by q , as used in tokamak related literature, is defined as $q = 1/\iota$. In addition, other parameters may have an influence on confinement properties of stellarators, such as the profile shape of ι . This parameter is called the magnetic shear. It seems that both low and high magnetic shear present good confinement qualities and these regions need to be explored [2]. For example, experimental studies at Wendelstein (W7-X) have shown a better confinement efficiency for high rotational transform values, provided that distinct optimum confinement windows close to low order resonances (1/3 and 1/2) were chosen [2, 4, 5]. Thus, a flat, shear-less profile is then desired to stay within the ι -range. More generally, we aim to understand which

combinations of magnetic axis torsion and flux surfaces ellipticity lead to shear-less profiles.

In light of that, it appears clear that stellarators optimisation is a tremendous task, and that one can only focus on certain *optimisation classes*. For instance, certain shear-less stellarators have shown quasi-axisymmetry [6], and thus it would be interesting to focus on confinement properties of shear-less stellarators, or to study the shear properties of quasi-axisymmetric stellarators.

Helander reviews in [1] that the rotational transform is affected by the ellipticity of the flux surfaces, the current introduced in the plasma, and the torsion of the magnetic axis, as in Eq.(28). Hence, part of this paper will focus mainly on the concept of torsion, mathematically, and then how the latter can generate something physical, as it acts on ι when added to the magnetic axis. Then, attention will be brought on the influence of ellipticity, by studying the magnetic shear.

Results obtained regarding the torsion from a mathematical point of vue are reviewed in III A. Behavior of the rotational transform, around the magnetic axis, is studied under certain circumstances in III B. Then, an analysis of the magnetic shear is reviewed under several combinations of torsion and ellipticity, in III C.

II. THEORY

A. Magnetic axis torsion from a mathematical point of view

One of the goals of this report is to study how the rotational transform is influenced by the torsion τ of the magnetic axis. Hence it is important to have a proper comprehension of the concept of torsion from a mathematical point of vue. Intuitively one can understand the torsion of a 3-dimensional curve as how much the latter bends to leave its osculating plane, that is the plane

* salomon.guinhardt@epfl.ch

[†] Swiss Plasma Center, Ecole Polytechnique Fédérale de Lausanne, Lausanne, Suisse

generated by \mathbf{T} and \mathbf{N} , the tangent and normal vectors respectively.

Let us now express τ in terms of the magnetic axis parametrisation, that we shall denote by \mathbf{r} . Assuming the curves later described to be closed, one can think of \mathbf{r} expressed as a function of a toroidal angle that we shall note ϕ . The torsion τ naturally arises from the Frenet-Serret formulas describing the evolution of the Frenet vectors \mathbf{T} , \mathbf{N} and \mathbf{B} , \mathbf{B} being the binormal vector [7]. Indeed, for a curve parametrised by its arc length l , one has the following system to describe the evolution of this set of vectors $\{\mathbf{T}, \mathbf{N}, \mathbf{B}\}$:

$$\frac{d\mathbf{T}}{dl} = \kappa \mathbf{N}, \quad (1)$$

$$\frac{d\mathbf{N}}{dl} = -\kappa \mathbf{T} + \tau \mathbf{B}, \quad (2)$$

$$\frac{d\mathbf{B}}{dl} = -\tau \mathbf{N}, \quad (3)$$

where κ denotes the curvature.

Now equipped with an expression linking the changes of $\{\mathbf{T}, \mathbf{N}, \mathbf{B}\}$ along the curve, one no longer needs to parametrise the curve by its arc-length. It is possible to express the above system as a function of another curve-parameter. Taking our toroidal ϕ introduced above as the parameter, that is $\mathbf{r} \equiv \mathbf{r}(\phi)$, one gets for the vectors $\{\mathbf{T}, \mathbf{N}, \mathbf{B}\}$:

$$\mathbf{T}(\phi) = \frac{\mathbf{r}'(\phi)}{\|\mathbf{r}'(\phi)\|}, \quad (4)$$

$$\mathbf{N}(\phi) = \frac{\mathbf{T}'(\phi)}{\|\mathbf{T}'(\phi)\|} = \frac{\mathbf{r}'(\phi) \times (\mathbf{r}''(\phi) \times \mathbf{r}'(\phi))}{\|\mathbf{r}'(\phi)\| \|\mathbf{r}''(\phi) \times \mathbf{r}'(\phi)\|}, \quad (5)$$

and

$$\mathbf{B}(\phi) = \mathbf{T}(\phi) \times \mathbf{N}(\phi). \quad (6)$$

Moreover, one obtains for the system (1) to (3):

$$\frac{d\mathbf{T}}{d\phi} = \|\mathbf{r}'\| \kappa \mathbf{N}, \quad (7)$$

$$\frac{d\mathbf{N}}{d\phi} = \|\mathbf{r}'\| (-\kappa \mathbf{T} + \tau \mathbf{B}), \quad (8)$$

$$\frac{d\mathbf{B}}{d\phi} = -\|\mathbf{r}'\| \tau \mathbf{N}. \quad (9)$$

Injecting the definitions (4), (5) and (6) in the system of equations (7) to (9), τ and κ read

$$\kappa = \frac{\|\mathbf{r}'(\phi) \times \mathbf{r}''(\phi)\|}{\|\mathbf{r}'(\phi)\|^3}, \quad (10)$$

$$\tau = \frac{\mathbf{r}'(\phi) \cdot (\mathbf{r}''(\phi) \times \mathbf{r}'''(\phi))}{\|\mathbf{r}'(\phi) \times \mathbf{r}''(\phi)\|^2}. \quad (11)$$

B. About SPEC

The Stepped Pressure Equilibrium Code (SPEC) [8], aims to determine 3D MHD equilibria, with a stepped pressure profile. It finds minimal plasma energy states conserving the constraints on ellipticity and fluxes in a set of N_V nested volumes $\{R_i\}$. To do so, the energy functional that needs to be minimised is the one introduced by M.J. Hole et al, [9]. The latter is the so-called the Multi-Region relaXed MHD (MRxMHD) energy-functional,

$$\mathcal{F} = \sum_{i=1}^{N_V} \left\{ \int_{R_i} \left(\frac{p}{\gamma - 1} + \frac{B^2}{2} \right) d\nu - \frac{\mu_i}{2} \left(\int_{R_i} \mathbf{A} \cdot \mathbf{B} d\nu - H_i \right) \right\}, \quad (12)$$

where p_i , H_i are the pressure and magnetic helicity in volume R_i . \mathbf{B} and \mathbf{A} are the magnetic field and vector potential respectively, η the adiabatic constant and $d\nu$ a differential volume element.

The calculus of variations for the functional \mathcal{F} yields to Euler-Lagrange equations for each volume R_i ,

$$\delta \mathcal{F} = 0 \implies \nabla \times \mathbf{B} = \mu_i \mathbf{B}. \quad (13)$$

Analytical resolution of Eq.(13) is done in Appendix (B), in the simple case of a screw pinch. Across each interface I_i , between volumes R_i and R_{i+1} , we ensure a force-balance condition, such that the total pressure (plasma and magnetic) is continuous:

$$\left[\left[p + \frac{B^2}{2} \right] \right] = 0. \quad (14)$$

In the particular case of $N_V = 1$, the energy states are the so-called Taylor states, while when $N_V \rightarrow \infty$, MRxMHD is equivalent to ideal MHD ones [10].

SPEC is a fixed boundary code and hence as any differential problem with fixed boundary conditions, it requires a specification of its boundary. That is achieved expressing the boundary of the plasma surface in terms of Fourier harmonics. The choice of cylindrical coordinates $\{\hat{\mathbf{R}}, \hat{\mathbf{Z}}\}$ enables to parametrise the boundary as follows:

$$\mathbf{S}(\theta, \phi) = R(\theta, \phi) \hat{\mathbf{R}} + Z(\theta, \phi) \hat{\mathbf{Z}} \quad (15)$$

where θ and ϕ are the poloidal and toroidal angles respectively, and range in $[0, 2\pi]$. R and Z are defined as truncated Fourier series:

$$R(\theta, \phi) = \sum_{m=0}^{M_{pol}} \sum_{n=-N_{tor}}^{N_{tor}} R_{mn} \cos(m\theta - nN_{fp}\phi), \quad (16)$$

$$Z(\theta, \phi) = \sum_{m=0}^{M_{pol}} \sum_{n=-N_{tor}}^{N_{tor}} Z_{mn} \sin(m\theta - nN_{fp}\phi), \quad (17)$$

where N_{fp} is the number of field periods. Let us point out that in the SPEC inputs used for computations below, R_{mn} is denoted by R_{nm} so this last notation will be kept for the results. Naturally, the same stands for Z_{mn} too.

The correspondance between cylindrical coordinates and cartesian ones can be made noting that

$$\hat{\mathbf{R}} = \cos(\phi)\hat{\mathbf{x}} + \sin(\phi)\hat{\mathbf{y}}, \quad (18)$$

and is important, since the curvature and hence the torsion, will be expressed in our numerical computations using the coordinate axis defined in terms of cartesian coordinates.

The SPEC solution then corresponds to the shapes of the interfaces $\{I_i\}$, and the magnetic field \mathbf{B} .

C. Magnetic axis torsion and rotational transform ι : without current and ellipticity

Let us define now the rotational transform. According to [11], ι can be defined as follows: the average angular advance of a field line poloidally each times it encircles the torus toroidally is $2\pi\iota$. This can be expressed mathematically as follows, with B^α the covariant components of \mathbf{B} :

$$\iota = \frac{\langle B^\theta \rangle}{\langle B^\phi \rangle} = \frac{\langle \mathbf{B} \cdot \nabla \theta \rangle}{\langle \mathbf{B} \cdot \nabla \phi \rangle} \quad (19)$$

Recall that the magnetic axis is described in cylindrical coordinates as

$$\mathbf{r}(\phi) = R(\phi)\hat{\mathbf{R}} + Z(\phi)\hat{\mathbf{Z}}. \quad (20)$$

Since the curve is $2\pi/N_{fp}$ periodic in ϕ , R and Z can be written as Fourier series:

$$R(\phi) = \sum_{n=0}^{N_{tor}} R_n \cos(nN_{fp}\phi), \quad (21)$$

$$Z(\phi) = \sum_{n=1}^{N_{tor}} Z_n \sin(nN_{fp}\phi). \quad (22)$$

So the coordinate vector, defined in cartesian coordinates can be expressed as

$$\mathbf{r} = R(\phi) \cos(\phi)\hat{\mathbf{x}} + R(\phi) \sin(\phi)\hat{\mathbf{y}} + Z(\phi)\hat{\mathbf{Z}}. \quad (23)$$

We are now in measure to express the torsion of the magnetic axis in terms of the formal derivatives of \mathbf{r} as it has been defined above. Recall indeed that

$$\tau = \frac{\mathbf{r}'(\phi) \cdot (\mathbf{r}''(\phi) \times \mathbf{r}'''(\phi))}{\|\mathbf{r}'(\phi) \times \mathbf{r}''(\phi)\|^2}. \quad (24)$$

Successive derivatives of Eq.(21)-(22) read:

$$\begin{aligned} \frac{d^k}{d\phi^k} R(\phi) &= R_{k\phi} \\ &= \mathcal{I}(k) \sum_{n=0}^{N_{tor}} R_n \cdot n^k \cdot N_{fp}^k \cdot \mathcal{F}_k(nN_{fp}\phi), \end{aligned} \quad (25)$$

$$\begin{aligned} \frac{d^k}{d\phi^k} Z(\phi) &= Z_{k\phi} \\ &= \mathcal{J}(k) \sum_{n=1}^{N_{tor}} Z_n \cdot n^k \cdot N_{fp}^k \cdot \mathcal{G}_k(nN_{fp}\phi), \end{aligned} \quad (26)$$

with $\mathcal{I}(k)$ and $\mathcal{J}(k)$ that can take values ± 1 , \mathcal{F}_k and \mathcal{G}_k being sin or cos, depending on the index k . Then Eq.(25)-(26) have been injected in Eq.(23)-(24), and implemented numerically. Note that the denominator of Eq.(24) is proportional to the curvature nominator squared κ^2 since the latter is expressed as

$$\kappa = \frac{\|\mathbf{r}'(\phi) \times \mathbf{r}''(\phi)\|}{\|\mathbf{r}'(\phi)\|^3}. \quad (27)$$

The previously introduced expression for τ can be then reused to compute the rotational transform ι as introduced by Helander in [1]:

$$\iota = \frac{1}{2\pi} \int_0^L \left[\frac{\mu_0 J}{2B_0} - (\cosh(\eta) - 1)d' - \tau \right] \frac{dl}{\cosh(\eta)} - N. \quad (28)$$

In Eq.(28), η characterises the ellipticity of magnetic surfaces, and J the current density on the axis, while d' corresponds to the angle between one of the semi axis of the ellipse centred at the coordinate axis, and the curvature vector, pointing in the normal direction. N is an integer discussed below. Hence, in the case of zero-current and ellipticity, those terms ought to be taken as zero and ι finally reads

$$\iota = \frac{1}{2\pi} \int_0^L -\tau dl - N, \quad (29)$$

which can be recast as

$$\iota = \frac{1}{2\pi} \int_0^{2\pi} -\tau \sqrt{R'(\phi)^2 + Z'(\phi)^2 + R(\phi)^2} d\phi - N, \quad (30)$$

taking account for the fact that the infinitesimal length element along the coordinates axis dl can be expressed in terms of $d\phi$, the variation of toroidal angle, through the jacobian (Appendix (C)). The signification of the $-N$ term will be discussed below.

Regarding the integer N in the expression (28), its meaning is somehow delicate, and it depends on the applied torsion. In order to understand it, one needs to consider the set of vectors $\{\mathbf{T}, \mathbf{N}, \mathbf{B}\}$, associated to the magnetic axis.

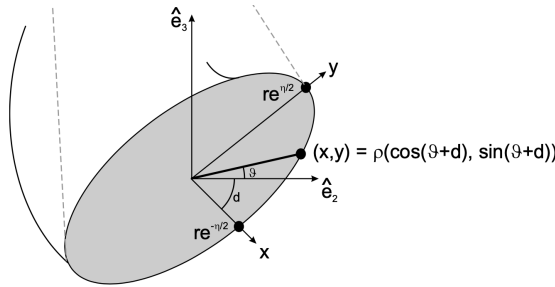


FIG. 1. Coordinates system $\{\mathbf{e}_1, \mathbf{e}_2, \mathbf{e}_3\} \equiv \{\mathbf{T}, \mathbf{N}, \mathbf{B}\}$ associated to magnetic axis: $\mathbf{e}_2 = \mathbf{N}$ is proportional to the curvature

Using the definition of the tangent vector $\mathbf{T} = dr/dl$ normalised, one gets

$$\mathbf{T} = \frac{1}{\sqrt{R'(\phi)^2 + Z'(\phi)^2 + R(\phi)^2}} \begin{pmatrix} R_\phi \\ R \\ Z_\phi \end{pmatrix}, \quad (31)$$

where the index ϕ means derivative with respect to ϕ and the above vector is expressed in the basis $\{\hat{\mathbf{R}}, \hat{\phi}, \hat{\mathbf{Z}}\}$. The normal vector \mathbf{N} is proportional to the derivative of \mathbf{T} with respect to a length element dl which can be rewritten as

$$\mathbf{N} \propto \frac{d\mathbf{T}}{dl} = \frac{1}{\sqrt{R_\phi^2 + Z_\phi^2 + R^2}} \frac{d\mathbf{T}}{d\phi}. \quad (32)$$

So finally

$$\mathbf{N} \propto \frac{1}{R_\phi^2 + Z_\phi^2 + R^2} \begin{pmatrix} R_{\phi\phi} - R \\ 2R_\phi \\ Z_{\phi\phi} \end{pmatrix} - \frac{R_\phi R_{\phi\phi} + RR_\phi + Z_\phi Z_{\phi\phi}}{(R_\phi^2 + Z_\phi^2 + R^2)^2} \begin{pmatrix} R_\phi - R \\ R \\ Z_\phi \end{pmatrix}. \quad (33)$$

N basically describes how many times the vector \mathbf{N} encircles the magnetic axis poloidally, during one toroidal turn. As introduced by mean of Fig.(4), the angle $\theta = 0$ defines a curve that we shall call C , and corresponds to the direction pointed by \mathbf{N} . In case of a plane magnetic axis, that is without any torsion, the curve C stays in the same plane, and hence does not encircle the magnetic axis poloidally. But C may encircle the magnetic axis an integer number of times N , in the case where torsion is added to the latter.

D. Magnetic shear

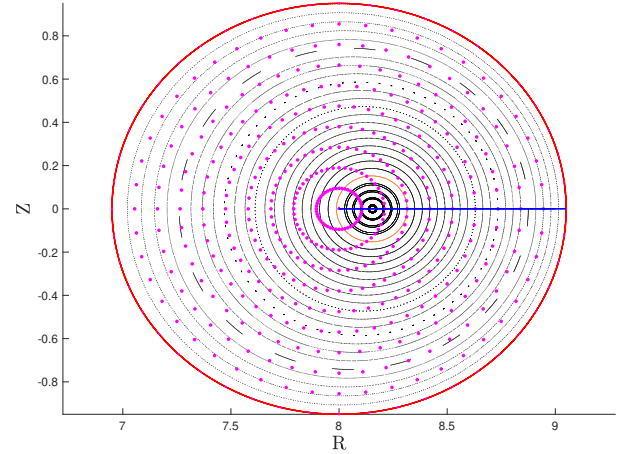


FIG. 2. Poincaré surfaces in the case of one volume, without current and ellipticity. Black surfaces correspond to magnetic surfaces. The grid of coordinates used by SPEC is shown in pink. The blue line is associated to the radial coordinate used in the calculus of the shear s .

Now that the rotational transform has been introduced mathematically, it can be interesting to focus on how the latter evolves, changing either the magnetic axis torsion, or the magnetic surfaces ellipticity, or both. This is done by mean of a dimensionless parameter, called the magnetic shear s . Formally, the magnetic shear is defined as the following ratio

$$s = \frac{r}{\iota} \frac{dl}{dr}, \quad (34)$$

where r is a radial coordinate. This way, we ensure that the magnetic shear describes the rate of change of ι following the radial coordinate, since $s \propto d\iota/dr$.

Analytical expressions of the magnetic shear, by mean of near-axis expansion, are tremendously difficult to obtain. In this work, we instead approach this question numerically with the SPEC code.

In SPEC, the coordinate axis does not necessarily coincide with the magnetic axis (see Fig.(2)). To determine ι , SPEC will use a *field-line tracing* algorithm, starting from the center of the coordinate grid (pink grid on Fig.(2)), and scanning toward its right till the boundary of the volume (red circle). Thus, to evaluate the derivative, the radial coordinate will be taken as on the blue line, thus $r \in [0, 1]$. The SPEC equilibrium from Fig.(2) has the rotational transform profile shown in Fig.(3).

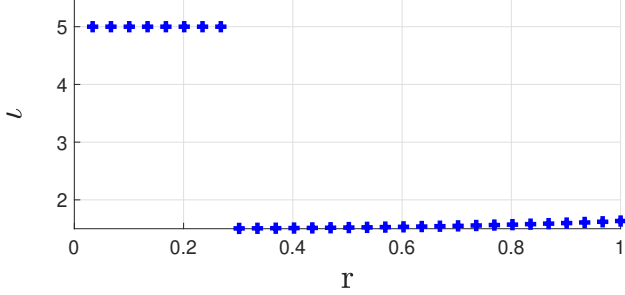


FIG. 3. Discontinuity in the ι profile for the volume of Fig.(2)

Regarding Fig.(3), it appears clearly that the first 8 points of the ι profile are erroneous, and will contribute to misrepresent the shear, since the discontinuity between the points 8 and 9 will lead to an error in the evaluation of the numerical derivative, although the first part shows a continuous trend. This wrong value for ι for these 8 points come from the fact that there is a shift between the coordinates grid used by SPEC and the poincare surfaces plotted in Fig.(2). Field lines that don't encircle the magnetic axis will give wrong ι values. Hence, it is necessary to take points such that their surface encircles the magnetic axis.

Thus one can note here that the coordinate axis, at the left end of the blue line, is first encircled by the Poincare surface 8, justifying that the first 8 points from the ι profile are not good to take. All points from index 9 till the end of the profile are good, but to make sure that the magnetic axis is not too decentred, a shift of 5 points is added, so the magnetic axis comes closer to the center of the next Poincare surfaces.

III. RESULTS

A. On the torsion from a mathematical point of vue

We first implement a code that solves Eq.(23)-(24) for any closed curve parametrised by $\mathbf{r}(\phi)$. We start by a

circular axis, with $R = R_0$, $Z = 0$ as in Fig.(4). As expected, for a circular axis, one observes a constant curvature and no torsion, since the axis does not leave the osculating plan at any time.

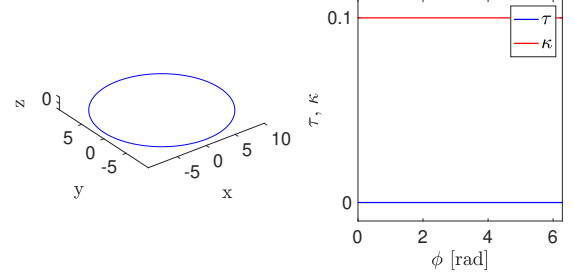


FIG. 4. Left: Circular magnetic axis - Right: Torsion and curvature. Note that as $R = 10$, $\kappa = 0.1 = 1/R$ as expected.

Now, the form of the axis has been changed to a toroidal helix, with $N_{fp} = 5$, and parametrised as

$$\begin{aligned} R(\phi) &= R_0 + R_{10} \cos(N_{fp}\phi), \\ Z(\phi) &= Z_{10} \sin(N_{fp}\phi). \end{aligned} \quad (35)$$

The major radius of the helix is R_0 and the minor radius, hence the torsion parameter, R_{10} following SPEC notation. This corresponds to the case that will be reviewed using SPEC in the following section. In SPEC parametrisations for ι studies, $R_{10} = Z_{10}$. Note that although the units (in caption of Fig.(5)) are not specified, it is of no particular importance since it is the ratio between R_0 and R_{10} that matters.

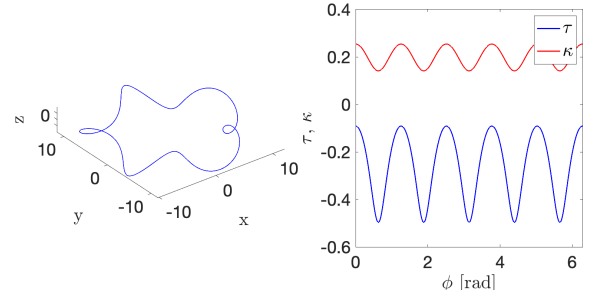


FIG. 5. Left: Toroidal-helical magnetic axis ($N_{fp} = 5$, $R_0 = 10$, $R_{10} = 2$) - Right: τ and κ .

Now, note that the curvature and the torsion are both non-constant and oscillating around a non-zero value. From now on, the average values, that is values around which κ and τ oscillate will be denoted by $\langle \cdot \rangle$ and defined as $\langle \cdot \rangle \equiv 1/2\pi \int_0^{2\pi} \cdot d\phi$. Thus, one sees that in the case of a toroidal helix with $N_{fp} = 5$ and $R_{10} = 1$, $\langle \tau \rangle < 0$.

Fig.(6) shows how the magnetic axis bends increasing the minor radius, as well as the behavior of the torsion in that case. One can then note that $\langle \tau \rangle$ increases with R_{10} , but diminishes in absolute value. It is important to

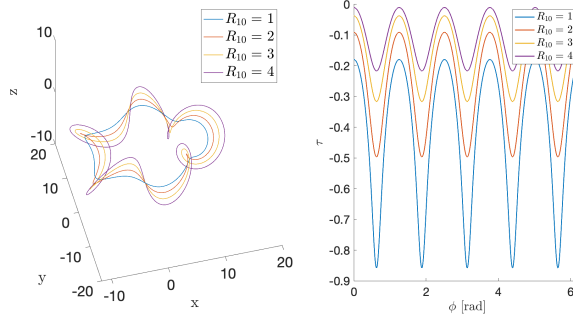


FIG. 6. Left: Magnetic axis - toroidal helix with increasing minor radius R_{10} - Left: τ in each case.

emphasise the fact that below a certain value of R_{10} , $\langle \tau \rangle$ is positive. The reason we observe the presence of this critical radius will be reviewed later. Nevertheless, it is observed that the average torsion goes to zero while the minor radius increases, as expected, since in the limit $R_{10} \rightarrow \infty$, the curve is locally similar as a circle with infinite radius.

B. Rotational transform in the case of torsion and no ellipticity

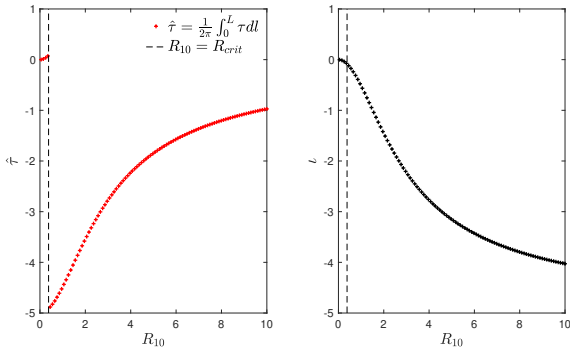


FIG. 7. Left: τ integrated along the axis - Right: ι from [1].

Now that τ has been numerically computed, we are now equipped with all that is needed to determine iota using eq.(28). Let us remind that in the case of zero-ellipticity and zero current, ι reads

$$\iota = -\frac{1}{2\pi} \int_0^L \tau dl - N. \quad (36)$$

Fig.(7) shows the result for the integral of τ along the magnetic axis, as well as the corresponding result for ι , increasing R_{10} . Note the discontinuity at $R_{10} \equiv$

$R_{crit} \simeq 0.38$. The torsion integrated along the magnetic axis is positive for $R_{10} < R_{crit}$, and is negative for $R_{10} > R_{crit}$. The rotational transform is nevertheless continuous, thanks to the proper value of N used in each $[0, R_{crit}]$ and $[R_{crit}, 10]$, as discussed below.

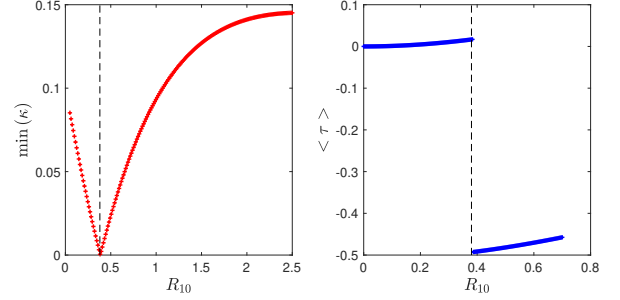


FIG. 8. Left: $\min(\kappa)$ increasing R_{10} , giving R_{crit} - Right: discontinuity in τ showing the existence of a critical radius R_{crit} .

The discontinuity in the torsion can be explained by the fact that it is inversely proportional to the curvature (see Eq.(24)), and that the latter has a minimum going to zero for $R_{10} \rightarrow R_{crit}$. Fig.(8) indeed shows that, and τ then agrees with the behaviour emphasised first in Fig.(6).

The reason why $\langle \tau \rangle$ is positive below R_{crit} and negative above is that there is a change of sign in the term $\mathbf{r}'(\phi) \cdot (\mathbf{r}''(\phi) \times \mathbf{r}'''(\phi))$ at R_{crit} . In fact τ can be rewritten as

$$\tau = \frac{1}{r'^6} \frac{\mathbf{r}' \cdot (\mathbf{r}'' \times \mathbf{r}''')}{\kappa^2}, \quad (37)$$

with κ the curvature. While κ goes to zero as R_{10} increases, $\|\tau\|$ increases since $\tau \propto \kappa^{-2}$. In fact, one could see the situation as follows, although the argument remains very qualitative:

To each of the radii R_0 and R_{10} can be associated a curvature vector, that is a normal direction. Each of them then contributes in κ a component κ_α , $\alpha = 0, 10$, that is

$$\kappa \equiv \kappa(\kappa_0, \kappa_{10}). \quad (38)$$

At R_{crit} , both components κ_α compensates exactly, and then one of the two becomes dominant as the roles changes.

As introduced in II C, the vector \mathbf{N} , pointing towards the direction of the curvature, corresponds to a curve winding (or not) around the magnetic axis. The number of times this curve encircles the magnetic axis has to be subtracted to the integral of τ along the axis, in order

to get ι . Regarding Fig.(9), the angle between the two components R and Z of $\mathbf{e}_2 = \mathbf{N}$ is represented along the magnetic axis, over a full toroidal period. One can then note that for $R_{10} \lesssim R_{crit}$, \mathbf{e}_2 does not rotate fully around the magnetic axis, whereas for $R_{10} \gtrsim R_{crit}$, it does N_{fp} times. This way, the value of N can be determined and ι as plotted in Fig.(7) can be obtained.

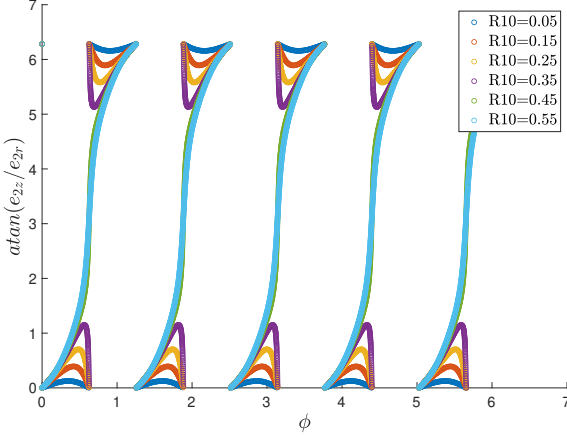


FIG. 9. Interval covered by the angle between the components r and z from the normal vector \mathbf{e}_2 . R_{10} ranges in an interval containing R_{crit} .

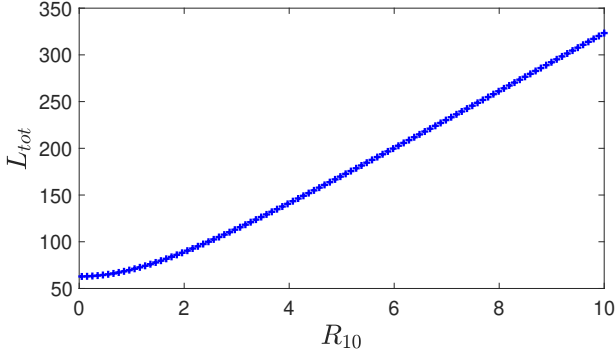


FIG. 10. Total magnetic axis length increasing R_{10} .

Figure.(10) represents the total length of the magnetic axis as a function of R_{10} . One sees that although the length tends to increase linearly, ι does not follow the same trend. Indeed, it has been shown that the average torsion tends to zero increasing the minor radius. So taking account for that, it is consistent that ι tends to get closer to the limit $\iota \rightarrow -5$ in the mathematical limit $R_{10} \rightarrow \infty \implies L \rightarrow \infty$.
Indeed,

$$\begin{aligned} R_{10} \rightarrow \infty \implies \langle \tau \rangle \rightarrow 0 \implies & \int_0^L \tau dl \rightarrow 0 \\ \implies \iota \rightarrow -N = -5. \end{aligned} \quad (39)$$

So until now, no inconsistency in the results has been observed, still taking account that the theoretical development for ι eq.(29) stands true close to the magnetic axis.

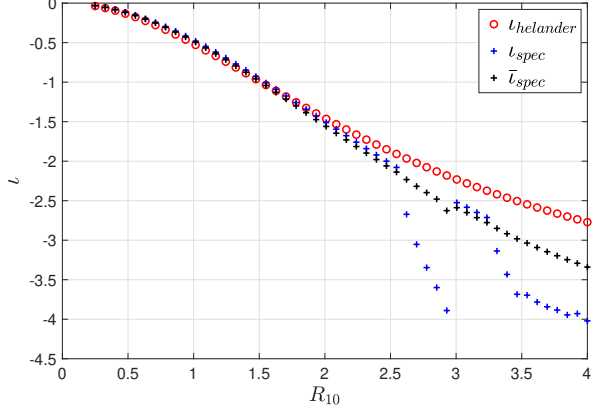


FIG. 11. Comparison of results for ι scanning over the torsion, and obtained from SPEC and Eq.(30).

Now, let us focus on how accurate ι evaluated from Eq.(29) is, comparing the above results with those obtained from SPEC from the same configuration. To do so the minor radius R_{10} has been scanned in the range $[0, 4]$, and the equilibrium has been determined by mean of the SPEC code, for 1 volume devoid of current and ellipticity.

Figure.(11) shows the result of the comparison. Note that SPEC gives a result for ι along a radial coordinate from the center to the boundary of the volume. Hence a particular value has to be chosen for ι_{SPEC} . It is not sufficient to take the first index, as explained in II D. So applying the procedure from II D, one gets the blue curve. Taking the average value of ι_{SPEC} along the volume-associated radial-coordinate yields to the black curve. It is observed that results for the expansion of ι as in eq.(29) show great concordance with SPEC results, as long as R_{10} does not reach too high values. Note how the points shift from the prediction (red) for large R_{10} .

To keep a high concordance between the two curves ι_{SPEC} and $\iota_{Helander}$ as R_{10} increases, it would be necessary to increase the Fourier/radial resolutions in SPEC. Moreover, as R_{10} reaches high values, during a toroidal step $d\phi$, the magnetic surface may be highly shifted in space, and hence, considering poincare plots along ϕ , one would observe that the coordinate axis moves a lot, hence making difficult to keep it centred. This might be partially improved by reducing the toroidal step $d\phi$, increasing the field-line tracing integrator precision. Nevertheless, one of the main results to keep in mind is that increasing R_{10} above the critical radius, increases τ , but decreases the latter in modulus. This leads to a decrease of ι towards the limit $\iota \rightarrow -N$.

C. Magnetic shear for several combinations of torsion and ellipticity

The goal here is to study the influence of several combinations of torsion and ellipticity, on the magnetic shear s . Recall that s is defined as follows:

$$s = \frac{r}{\iota} \frac{d\iota}{dr}, \quad (40)$$

with r a radial coordinate. As it has been shown in the previous sections, the torsion is changed by R_{10} and the ellipticity by the second mode R_{11} . We performed a scan of the configuration space $R_{10} = Z_{10}$, $R_{01} = Z_{01}$ and $R_{11} = Z_{11}$.

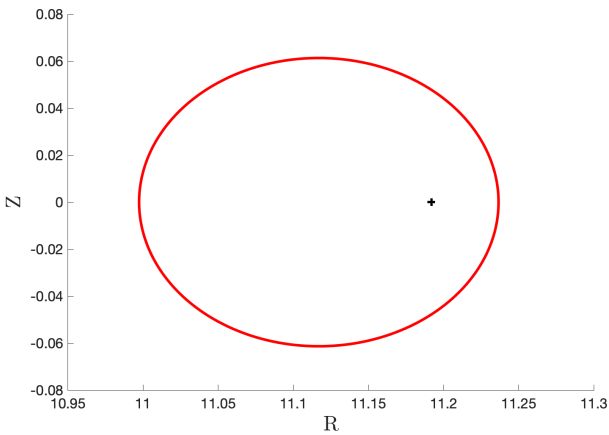


FIG. 12. First Poincare surface encircling the magnetic axis, giving the index of the first ι_{SPEC} term to take into account for the shear.

Fig.(12) shows the representation of the first flux-surface that encircles the magnetic axis, for a specific equilibrium. Note that although inside the surface, the magnetic axis is still decentred. Thus, the index of the flux-surface drawn here was raised of a certain shift $n_{shift} = 5$. Then, all points form the iota profiles as the one drawn in Fig.(3), *from the shifted index* were considered in order to evaluate the derivative from Eq.(40), as explained in II D.

To evaluate the proper behaviour of s under several couples (R_{10}, R_{11}) , 6500 SPEC-equilibria were considered, with $R_{10} \in [-2, 2]$ and $R_{11} \in [0.05, 0.5]$, with 100 points in each direction, giving a step of $\Delta R_{10} = 4 \cdot 10^{-2}$ and $\Delta R_{11} = 45 \cdot 10^{-4}$. The result for $s(R_{10}, R_{11})$ is shown in Fig.(13).

Note that Fig.(13) only focuses on the region of interest, so $R_{10} \lesssim 1.2$ and $R_{11} \lesssim 0.34$. Other regions of interest could lie outside this range, and will be explored in future work. The red curve corresponds to

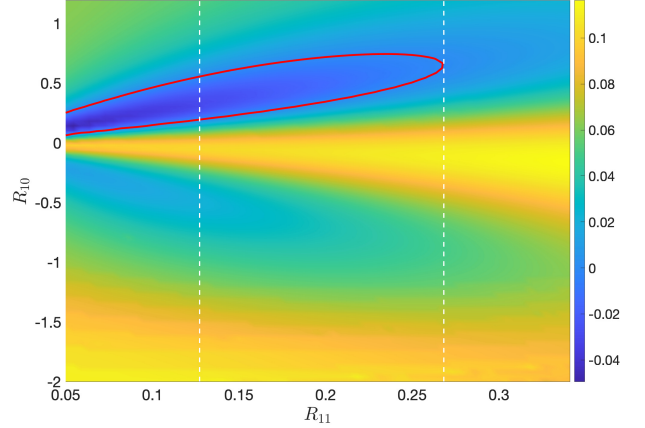


FIG. 13. Magnetic shear s scanned over different combinations of torsion and ellipticity, that is different couples $(\tau, \eta) \leftrightarrow (R_{10}, R_{11})$.

the level set $S \equiv \{s = 0\}$, while the two white dashed-lines corresponds to two fixed R_{11} values, $R_{11}^1 = 0.1273$ and $R_{11}^2 = 0.2828$ respectively, chosen since their intersection with S is non empty. We will denote by $d_i \equiv \{R_{11} = R_{11}^i\}$. Thus the above condition read

$$d_i \cap S \neq \emptyset. \quad (41)$$

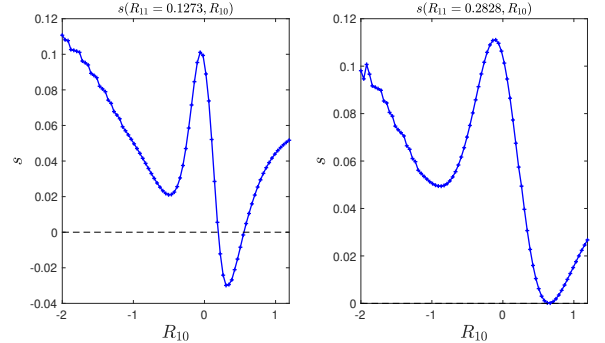


FIG. 14. Profiles of the magnetic shear varying τ for 2 fixed ellipticity values η_i , $i = 1, 2$ (fixed R_{11}), i.e profiles of s along d_i

The magnetic shear has been plotted for the two sets d_i , $i = 1, 2$. The results appear on Fig.(14). It appears that in the region of weak ellipticity, for low R_{11} , s shows steeper variations than for larger ellipticity, varying τ . One can remark, from Fig.(13) that the shear-less zone extends over an R_{10} range containing the critical radius. The shear is higher at almost zero torsion ($R_{10} \sim 0$), no matter what the ellipticity is.

It is interesting to focus on two specific couples (τ, η) , close to the set S . We chose them in the set d_1 . The two couples are represented in lower part of Fig.(15).

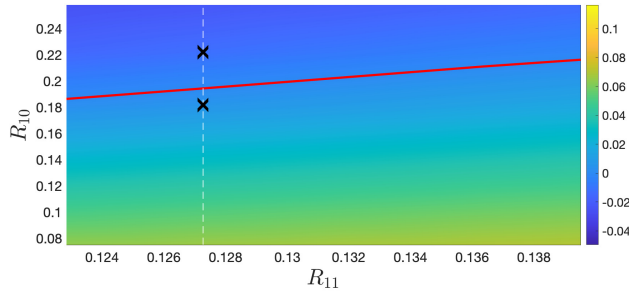


FIG. 15. Two specific couples (R_{10}, R_{11}) both with shear above and below zero.

Their ι -profiles have been plotted in Fig.(16). The curve ι_b corresponds to the couple below the S –curve, hence showing an increasing profile (positive shear). Inversely, ι_a corresponds to the couple above the S –curve, with $s \leq 0$. Note that both profile show a very low shear, confirming that the set S is relevant.

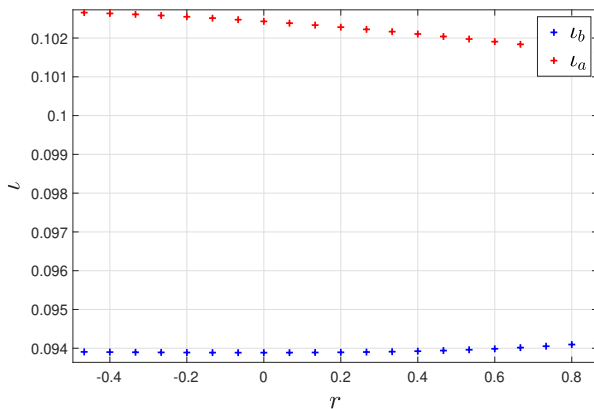


FIG. 16. ι -profiles for the two couples (R_{10}, R_{11}) from Fig.(15). The red one corresponds to $s < 0$ and the blue one to $s > 0$.

Some configurations of quasi-axisymmetric stellarators have shown a shear almost constantly zero [12]. Similar properties have been observed for quasi-helically symmetric configurations. Thus, it can be interesting to see whether a configuration (τ, η) shows such properties as a magnetic field independent of the toroidal angle for example.

Fig.(17) shows the magnitude of the magnetic field at the boundary of the volume for a configuration in S . One can observe that the modulus of \mathbf{B} has a periodicity of 5 maxima over a full toroidal turn, corresponding to $N_{fp} = 5$.

Nevertheless, it is not possible by mean of only this result to conclude on the quasi-symmetry of such a con-

figuration, since one has to plot the magnitude of \mathbf{B} as a function of the Boozer coordinates. This will be explored in a future work.

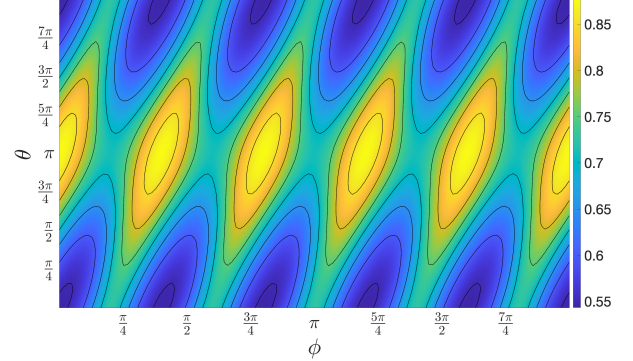


FIG. 17. Modulus of the magnetic field $\|\mathbf{B}\|$ at the boundary of the volume as a function of the toroidal and poloidal angles ϕ and θ for a point located on the curve $s \equiv 0$.

IV. CONCLUSION

In this report, some general characteristics of the mathematical concept of torsion have been reviewed. Behaviour of the latter in the simple case of a circular axis, as well as of a toroidal helix has been studied. Numerical simulations were performed in order to determine the rotational transform at the magnetic axis in the case of a toroidal helix with $N_{fp} = 5$, and varying the minor radius.

The results obtained have been compared to those obtained running the SPEC code, with one volume, no current and no ellipticity. Results have shown a great concordance with predicted results, confirming Helander's derivation in that specific case. One could contemplate doing further tests, adding current and magnetic surfaces ellipticity to expression (28), for example.

Attention has then been drawn on the magnetic shear, since it is a promising parameter to take into account in several optimisation strategies. The magnetic shear in a single volume, devoid of current, and under several torsion and ellipticity combinations has been computed, and high shear regions as well as shear-less ones have been emphasised. It could be interesting to run tests to show whether such configurations with high or low shear present hidden symmetries such as quasi-axisymmetry or quasi-helical symmetry, since some of these configurations might exhibit MHD-stability [12, 13].

Appendix A: MHD equilibrium in a screw pinch

From the ideal MHD equation

$$\mathbf{j} \times \mathbf{B} = \nabla p, \quad (\text{A1})$$

and assuming the plasma pressure and the rotational transforms are known, the goal is to show that in cylindrical geometry

$$\frac{d}{dr} \left\{ p + \left(1 + \frac{\iota^2 r^2}{R_0^2} \right) \frac{B_z^2}{2\mu_0} \right\} + \frac{r B_z^2 \iota^2}{R_0^2 \mu_0} = 0. \quad (\text{A2})$$

Using the axisymmetry of the system, one gets that the partial derivatives according to the height and angle in the cylinder vanish, that is

$$\frac{\partial}{\partial \theta} = \frac{\partial}{\partial z} = 0. \quad (\text{A3})$$

From now on, all the derivatives will be written the following way, for the sake of simplicity:

$$\frac{\partial}{\partial \alpha} = \partial_\alpha \quad \text{and} \quad \frac{d}{d_\alpha} = d_\alpha \quad \alpha = r, z\theta. \quad (\text{A4})$$

$$\begin{aligned} \iota &= \frac{1}{2\pi} \int_0^{2\pi R_0} \frac{d\theta}{dz} = \frac{1}{2\pi} \int_0^{2\pi R_0} \frac{B_\theta}{r B_z} dz \\ &= \frac{2\pi R_0}{2\pi r} \frac{B_\theta}{B_z}. \end{aligned} \quad (\text{A5})$$

So one gets for ι^2 :

$$\iota^2 = \frac{R_0^2 B_\theta^2}{r^2 B_z^2}. \quad (\text{A6})$$

Taking into account the two following Maxwell equations

$$\nabla \times \mathbf{B} = \mu_0 \mathbf{j}, \quad (\text{A7})$$

$$\nabla \cdot \mathbf{B} = 0, \quad (\text{A8})$$

the ideal MHD equation A1 reads

$$(\nabla \times \mathbf{B}) \times \mathbf{B} = \mu_0 \mathbf{j}. \quad (\text{A9})$$

But

$$\begin{aligned} \nabla \times \mathbf{B} &= \begin{pmatrix} \frac{1}{r} \partial_\theta B_z - \partial_z B_\theta \\ \partial_z B_r - \partial_r B_z \\ \frac{1}{r} \partial_r (r B_\theta) - \frac{1}{r} \partial_\theta B_r \end{pmatrix} \\ &= \begin{pmatrix} 0 \\ -\partial_r B_z \\ \frac{1}{r} \partial_r (r B_\theta) \end{pmatrix}, \end{aligned} \quad (\text{A10})$$

and

$$\nabla p = \begin{pmatrix} \partial_r p = d_r p \\ \frac{1}{r} \partial_\theta p = 0 \\ \partial_z p = 0 \end{pmatrix}. \quad (\text{A11})$$

So we are only interested in computing the radial part of Eq.(A9).

$$\begin{aligned} (\nabla \times \mathbf{B}) \times \mathbf{B} &= \begin{pmatrix} 0 \\ -\partial_r B_z \\ \frac{1}{r} \partial_r (r B_\theta) \end{pmatrix} \times \begin{pmatrix} 0 \\ B_\theta \\ B_z \end{pmatrix} \\ &= \begin{pmatrix} -B_z \partial_r B_z - \frac{1}{r} \partial_r (r B_\theta) B_\theta \\ \dots \\ 0 \end{pmatrix}, \end{aligned} \quad (\text{A12})$$

which yields to (since the magnetic field components are only radial dependent)

$$\mu_0 d_r p + B_z d_r B_z + B_\theta \frac{1}{r} d_r (r B_\theta) = 0. \quad (\text{A13})$$

Moreover,

$$B_z d_r B_z = \frac{1}{2} d_r (B_z^2), \quad (\text{A14})$$

and

$$B_\theta \frac{1}{r} d_r (r B_\theta) = \frac{1}{r} B_\theta^2 + \frac{1}{2} d_r B_\theta^2. \quad (\text{A15})$$

Hence, Eq.(A13) reads:

$$\mu_0 d_r p + \frac{1}{2} d_r \{ B_z^2 + B_\theta \} + \frac{1}{r} B_\theta^2. \quad (\text{A16})$$

It is also convenient to write the angular components B_θ as a function of B_z using the definition of ι :

$$\frac{B_\theta^2}{2\mu_0} = \frac{\iota^2 r^2 B_z^2}{2\mu_0 R_0^2}, \quad (\text{A17})$$

as well as

$$\frac{1}{r\mu_0} B_\theta^2 = \frac{\iota^2 r B_z^2}{\mu_0 R_0^2}. \quad (\text{A18})$$

This way, one finally gets to the desired result:

$$\frac{d}{dr} \left\{ p + \left(1 + \frac{\iota^2 r^2}{R_0^2} \right) \frac{B_z^2}{2\mu_0} \right\} + \frac{r B_z^2 \iota^2}{R_0^2 \mu_0} = 0. \quad (\text{A19})$$

Appendix B: Magnetic field solution in nested flux surfaces

Starting from the Maxwell equation Eq.(B1)

$$\nabla \times \mathbf{B} = \mu_0 \mathbf{j}, \quad (\text{B1})$$

and imposing

$$\mu_0 \mathbf{j} = \mu \mathbf{B}, \quad (\text{B2})$$

as we desire to solve this equation in a screw pinch, one gets the following

$$\nabla \times \mathbf{B} = \mu \mathbf{B}. \quad (\text{B3})$$

Using the rotational definition Eq.(A10), one gets the following set of equations to solve:

$$\begin{aligned} \nabla \times \mathbf{B} &= \begin{pmatrix} \frac{1}{r} \partial_\theta B_z - \partial_z B_\theta \\ \partial_z B_r - \partial_r B_z \\ \frac{1}{r} \partial_r (r B_\theta) - \frac{1}{r} \partial_\theta B_r \end{pmatrix} \\ &= \begin{pmatrix} \mu B_r \\ \mu B_\theta \\ \mu B_z \end{pmatrix} \\ &= \mu \mathbf{B}. \end{aligned} \quad (\text{B4})$$

Using the axisymmetry of the system, the radial component of Eq.(B4) yields to

$$B_r = 0, \quad (\text{B5})$$

while along θ it becomes

$$\begin{aligned} \partial_z B_r - \partial_r B_z &= -\partial_r B_z \\ &= \mu B_\theta \iff B_\theta = -\frac{1}{\mu} \partial_r B_z. \end{aligned} \quad (\text{B6})$$

So B_z needs to be determined in order to find B_θ . Projecting Eq.(B4) along z :

$$\frac{1}{r} \partial_r (r B_\theta) - \frac{1}{r} \partial_\theta B_r = \mu B_z \iff \frac{1}{r} \partial_r (r B_\theta) = \mu B_z. \quad (\text{B7})$$

Developing the above derivative and replacing B_θ from Eq.(B6)

$$B_\theta = -\frac{1}{\mu^2} \partial_r \left\{ -\frac{1}{r^2} B_\theta + \frac{1}{r} \partial_r B_\theta + \partial_{r^2}^2 B_\theta \right\}, \quad (\text{B8})$$

which is equivalent to the following

$$r^2 \partial_{r^2}^2 B_\theta + r \partial_r B_\theta + (\mu^2 r^2 - 1) B_\theta = 0. \quad (\text{B9})$$

This last equation can be cast in the form a Bessel equation by mean of a variable change

$$x = \mu r \implies \partial_r = \partial_x x \cdot \partial_x, \quad (\text{B10})$$

yielding to

$$x^2 \frac{\partial^2}{\partial x^2} B_\theta + x \frac{\partial}{\partial x} B_\theta + (x^2 - 1) B_\theta = 0, \quad (\text{B11})$$

which has as a solution a first order Bessel function J_1 , that is $B_\theta(x(r)) = J_1(x(r))$.

Appendix C: Derivation of $dl(d\phi)$

Recall that the coordinates axis is expressed as follows:

$$\mathbf{r}(\phi) = R(\phi) \hat{\mathbf{R}} + Z(\phi) \hat{\mathbf{Z}}. \quad (\text{C1})$$

So using Poisson's rule:

$$\frac{d\hat{\mathbf{R}}}{d\phi} = \hat{\mathbf{Z}} \times \hat{\mathbf{R}} = \hat{\phi}. \quad (\text{C2})$$

So the differential $d\mathbf{r}$ reads

$$d\mathbf{r} = \frac{\partial \mathbf{r}}{\partial \phi} d\phi = \left(R'(\phi) \hat{\mathbf{R}} + R(\phi) \hat{\phi} + Z'(\phi) \hat{\mathbf{Z}} \right) d\phi, \quad (\text{C3})$$

and hence

$$dr = (d\mathbf{r} \cdot d\mathbf{r})^{\frac{1}{2}} = \sqrt{R'(\phi)^2 + Z'(\phi)^2 + R(\phi)^2} d\phi. \quad (\text{C4})$$

-
- [1] Per Helander, "Theory of plasma confinement in non-axisymmetric magnetic fields" 2014 Rep. Prog. Phys. 77 087001, <https://doi.org/10.1088/0034-4885/77/8/087001>
- [2] Ascasibar, Enrique, Lopez-Bruna, Daniel, and Castejon, Francisco. "Effect of Rotational Transform and Magnetic Shear on Confinement of Stellarators", in Plasma and Fusion Research · January 2008, <https://doi.org/10.1585/PFR.3.S1004>
- [3] D.A. Gates et al, "Recent advances in stellarator optimization", 2017 Nucl. Fusion 57 126064, <https://doi.org/10.1088/1741-4326/aa8ba0>
- [4] H. Ringler et al., "Plasma Physics and Controlled Nuclear Fusion Research", 32, 933 (1990)
- [5] R.Brakel et al, "Proc. 20th EPS Conf". (Lisbon), 361, (1993)
- [6] Matt Landreman, Elizabeth Paul. "Magnetic fields with precise quasisymmetry for plasma confinement". [physics.plasm-ph] <https://arxiv.org/abs/2108.03711>
- [7] Mate, Attila. "The Frenet-Serret Formulas." Brooklyn Collage Of The City University Of New York, izdano 19 (2017).
- [8] S. R. Hudson, R. L. Dewar, G. Dennis, et al. Phys. "Computation of multi-region relaxed magnetohydrodynamic equilibria". Plasmas 19, 112502 (2012); <https://doi.org/10.1063/1.4765691>
- [9] Phys. Plasmas 19, 112502 (2012); <https://doi.org/10.1063/1.4765691>
- [10] SPEC - Stepped Pressure Equilibrium Code: Algorithm <https://w3.ppl1.gov/~shudson/Spec/Algorithm.pdf>
- [11] Allen H. Boozer , "What is a stellarator?", Physics of Plasmas 5, 1647-1655 (1998) <https://doi.org/10.1063/1.872833>
- [12] S. A. Henneberg, M. Drevlak, C. Nührenberg, C. D. Beidler, Y. Turkin, J. Loizu, P. Helander "Properties of a new quasi-axisymmetric configuration" <https://doi.org/10.1088/1741-4326/aaf604>
- [13] Cooper, W A, Isaev, M, Leneva, A E, Mikhailov, M, Shafranov, V D, and Subbotin, A A. "Optimisation of stellarator systems: Possible ways". IAEA: N. p., 2001. Web.